



HAL
open science

Development of the curvilinear coordinate method for the computation of quasi-static fields induced by an eddy current probe scanning a 3D conductor of complex shape characterized by an arbitrary 2D surface

Denis Prémel, G. Granet

► To cite this version:

Denis Prémel, G. Granet. Development of the curvilinear coordinate method for the computation of quasi-static fields induced by an eddy current probe scanning a 3D conductor of complex shape characterized by an arbitrary 2D surface. *International Journal of Numerical Modelling: Electronic Networks, Devices and Fields*, 2018, 31 (2), 10.1002/jnm.2219 . cea-01764698

HAL Id: cea-01764698

<https://cea.hal.science/cea-01764698>

Submitted on 6 Feb 2024

HAL is a multi-disciplinary open access archive for the deposit and dissemination of scientific research documents, whether they are published or not. The documents may come from teaching and research institutions in France or abroad, or from public or private research centers.

L'archive ouverte pluridisciplinaire **HAL**, est destinée au dépôt et à la diffusion de documents scientifiques de niveau recherche, publiés ou non, émanant des établissements d'enseignement et de recherche français ou étrangers, des laboratoires publics ou privés.

Development of the curvilinear coordinate method for the computation of quasi-static fields induced by an Eddy Current probe scanning a 3D conductor of complex shape characterized by an arbitrary 2D surface

D. PRÉMEL^{*1} and G. GRANET²

¹CEA LIST, Laboratoire de Simulation et de Modélisation en Électromagnétisme, 91191 Gif-sur-Yvette, France

²Institut Pascal, Université Blaise Pascal, 63006 Clermont-Ferrand, France

Abstract

This paper deals with the development of a semi-analytical model for the fast computation of the quasi-static field induced by any Eddy Current probe in a 3D conductor of complex shape. The workpiece is considered as a planar half-space mock-up with an interface air-conductor characterized by an arbitrary 2D surface $a(x, y)$. The curvilinear coordinate method consists in introducing a change of coordinates in order to be able to write analytically and easily the boundary conditions at the interface air-metal. Due to the novel generalized metric space, the covariant form of Maxwell's equations must be considered. The Curvilinear Coordinate Method (CCM) is widely used in the optical community for the analysis the diffraction phenomenon on gratings. The method has been applied recently for Eddy Current calculations in the planar case for 2.5D configurations characterized by a 3D eddy current probe and a 2D layered stratified conducting media. By an extension to 3D problems, this work constitutes the preliminary task for the development of a complete numerical model which has the capability to address very complex Eddy Current Non-Destructive Testing (ECNDT) configurations such as a stratified layered media constituted by a set rough interfaces. For that purpose, the modal formalism is described for the first time in the 3D case and several numerical experiments show the validity and the efficiency of the fast numerical model in comparison to the Finite Element method.

1 Introduction

The fast computation of the response of a 3D eddy current probe scanning any homogeneous conductor of complex shape presents a kind of challenge in Eddy Current Non-Destructive Testing (ECNDT)

*E-Mail: denis.premel@cea.fr

community. Without speaking about the response of the EC sensor due to a tiny flaw such as a crack or a notch, it is often required to compute the response of the probe due to some local variations of the geometry of the workpiece. For instance, during any inspection procedure, some corrosion defect may be represented by variations of the thickness of layers in aircraft lap joints. Since, the change in the impedance of the EC probe may be calculated by using the Auld's formula and the reciprocity principle, it is necessary to compute as quickly as possible the tangential components of the quasi-static electric and magnetic field at the air-metal interface. The Curvilinear Coordinate Method (CCM) is particularly effective for this work since these tangential components are forwardly obtained when writing analytically the boundary conditions at the desired interface. Indeed, this approach is based on a specific change of coordinates which is called the translation system of coordinates which is non necessary orthogonal. Though this method is very popular, in the optical domain, for the computation of the fields scattered by 2D diffraction gratings [1] or by perfectly conducting random surfaces [2] enlightened by a plane wave it is less known in the low frequency community. To the best of our knowledge, the CCM was used for the first time in 2008 by D.Prémel in a preliminary study for a 2D eddy current problem [3]. Then, it has been employed for simulating a first 2.5D ECNDT configuration [4] before developing more practical cases of interest: a 3D EC probe scanning a 2D multilayered conductor with parallel [5] or non-parallel interfaces [6]. The purpose of the present paper is to address the following 3D problem: a 3D EC probe scanning a 3D conductor of complex shape presenting a rough interface varying along the two directions x and y and described by any analytical equation $z = a(x, y)$ (see figure 1). In contrast to purely numerical models which require a mesh of the workpiece, CCM can provide a semi-analytical model by using a modal decomposition of the tangential components of the electromagnetic field which depends on the surface itself. The originality of this method precisely lies in the fact that the modal decomposition is specifically linked to a change of coordinates which induce a metric tensor obtained in some analytical manner. In a previous work, the tangential components of the field were reconstructed from two auxiliary potentials by introducing as usual a second order vector potential formulation [7]. In the present paper, the formulation is very similar to what is done in waveguide theory where the tangential components (the so-called transverse components in the waveguide context) components are reconstructed from two scalar potentials which are the two longitudinal components of the fields. The key of this method is to derive the modal expansions of the two scalar potentials. It has to be emphasized that the sought eigenfunctions depend on the metric tensor describing the local variations of the geometry. Modal solutions are numerically obtained in the 2D Fourier space by solving a generalized eigenvalue algebraic equation deduced from the wave equation satisfied by the two potentials. The main difficulty of the numerical problem lies in obtaining of the eigenvalue matrix due to the truncation, in some practical case of the Fourier domain. This point will be particularly discussed in this paper. Anyway, solving the eigenproblem represents the most time-consuming step of the new developed code. This paper is organized as follows. The CCM is firstly described for 2D arbitrary interfaces $a(x, y)$. Maxwell's equations are written under the covariant form with the coefficients of the metric tensor the new non-orthogonal coordinates. A TE/TM decomposition is then derived with the longitudinal covariant components of the electromagnetic field as generating functions. The eigenvalue problem is numerically solved by

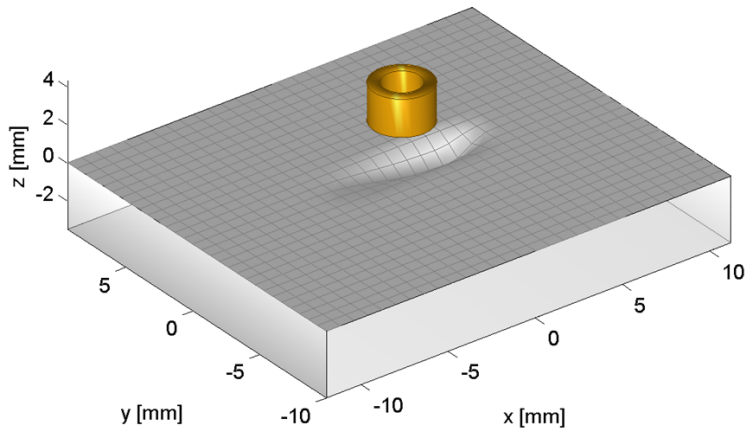


Figure 1: A 3D EC probe is scanning a conductive slab with a rough interface varying along the two directions x and y .

using the method of moments in the spectral domain. Boundary conditions are then introduced in order to find numerically the coefficients of the modal expansion of the two potentials. Some numerical experiments show the validity of the numerical model and some simulated data obtained from a Finite Element (FE) commercial software are compared to data provided by the resulting numerical model. The cartography of the tangential components are displayed for one position of the EC probe before presenting finally the change of the impedance of the EC probe when scanning the 2D perturbed surface. The current limitations of the method due to the truncation of eigensolutions in the Fourier domain and to the requirement in term of memory space are discussed. The paper is closed by some conclusions, remarks and perspectives for the future.

2 Physical formalism of the problem

In this section, we recall the 3D formalism of the C-Method which comes from the optical domain but it must be translated in our context. The main problem consists in obtaining the modal decomposition of the tangential components of the field on each interface taking into account the novel metric tensor resulting from the change of coordinates.

2.1 Change of coordinate system

Let us consider a homogeneous conductive slab presenting a 2D rough interface varying along the two axis x and y described by an arbitrary analytical equation $z = a(x, y)$ (see figure 1). In this figure, the rough surface is separating two media, the air domain above and the conductor one below. The current medium will be denoted by the index p in the following ($p = 0, 1$). In this example, the EC

probe is an air-core probe of cylindrical shape but its may be rectangular, D-shaped or a meander one since boundary conditions include the values of the tangential components of the electromagnetic field at the interface provided by any kind of air-core coil. The introduction of a ferrite core will require more developments in order to take into account coupling effects, one principle solution is described in the reference [8]. Let us apply the following non-orthogonal translation coordinates system:

$$\begin{cases} x = x^1 \\ y = x^2 \\ z = x^3 + a(x^1, x^2). \end{cases}, \quad (1)$$

In this new coordinate system, the interface fits a coordinate surface. Thus, writing boundary conditions at the interface becomes easier since it amounts to write four equalities at $x^3 = 0$. However, Maxwell's equations become more complicated because the covariant form of Maxwell's equations which does not depend on the choice of coordinate system [9] must be used for taking into account the novel metric tensor. Indeed, considering a map from a cartesian coordinate system $\{x, y, z\}$ to a new coordinate system $\{x^1, x^2, x^3\}$ the jacobian transformation matrix \mathbf{J} is for instance given in [10]:

$$\mathbf{J} = \begin{bmatrix} \frac{\partial x}{\partial x^1} & \frac{\partial x}{\partial x^2} & \frac{\partial x}{\partial x^3} \\ \frac{\partial y}{\partial x^1} & \frac{\partial y}{\partial x^2} & \frac{\partial y}{\partial x^3} \\ \frac{\partial z}{\partial x^1} & \frac{\partial z}{\partial x^2} & \frac{\partial z}{\partial x^3} \end{bmatrix} = \begin{bmatrix} 1 & 0 & 0 \\ 0 & 1 & 0 \\ \dot{a}_1 & \dot{a}_2 & 1 \end{bmatrix} \quad (2)$$

where it is assumed that $a(x, y) = a(x^1, x^2)$ is a differentiable function according to the two directions x and y . Let us denote by $\dot{a}_1 = \partial_x a$ and $\dot{a}_2 = \partial_y a$ the partial derivatives. Since \mathbf{J}^t stands for the transposed matrix of \mathbf{J} , the tensor metric $g_{ij} = \mathbf{J}^t \mathbf{J}$ and the conjugate tensor metric $g^{ij} = [g_{ij}]^{-1}$ are given by:

$$g_{ij} = \begin{bmatrix} 1 + \dot{a}_1^2 & \dot{a}_1 \dot{a}_2 & \dot{a}_1 \\ \dot{a}_1 \dot{a}_2 & 1 + \dot{a}_2^2 & \dot{a}_2 \\ \dot{a}_1 & \dot{a}_2 & 1 \end{bmatrix}, \quad [g^{ij}] = \begin{bmatrix} 1 & 0 & -\dot{a}_1 \\ 0 & 1 & -\dot{a}_2 \\ -\dot{a}_1 & -\dot{a}_2 & 1 + \dot{a}_1^2 + \dot{a}_2^2 \end{bmatrix} = \begin{bmatrix} 1 & 0 & g^{13} \\ 0 & 1 & g^{23} \\ g^{13} & g^{23} & g^{33} \end{bmatrix} \quad (3)$$

The determinant g of g_{ij} is $g = |g_{ij}| = 1$. In this natural coordinate system, the covariant components of the electrical (magnetic) field E_1, E_2 (H_1, H_2) corresponds to the tangential components of the electrical (magnetic) field.

2.2 Covariant form of Maxwell's equations

According to E. Post [9] and assuming a time dependence $e^{i\omega t}$, the complex amplitudes of the covariant components of the electrical and the magnetic fields, respectively denoted by E_i and H_i are linked by Maxwell's equations:

$$\begin{cases} \xi^{i,j,k} \partial_j E_k & = -i\omega \mu_0 \mu_p \sqrt{g} g^{ij} H_j \\ \xi^{i,j,k} \partial_j H_k & = i\omega \varepsilon_0 \varepsilon_p \sqrt{g} g^{ij} E_j \end{cases}, \quad \{i, j, k\} \in \{1, 2, 3\} \quad (4)$$

where ε_0 and μ_0 stand for the vacuum magnetic permeability and the vacuum dielectric permittivity and ε_p and μ_p stand for the relative magnetic permeability and the relative dielectric permittivity of the medium p . Since the conductivity of the medium is denoted by σ_p , its relative permittivity may be a complex number given by $\varepsilon_p = 1 - \frac{i\sigma_p}{\omega\varepsilon_0}$. ∂_j denotes the partial derivative operator with respect to the variable x^j and $\xi^{i,j,k}$ denotes the Lévi-Civita indicator [11]. By an observation of these equations, it is important to note that even if the medium is a homogeneous one, changing the coordinates system leads to substitute the initial electromagnetic properties of the medium by an electrical and permittivity tensor $\bar{\varepsilon} = \varepsilon_0\varepsilon_p\sqrt{g} g^{ij}$ and a magnetic permeability tensor $\bar{\mu} = \mu_0\mu_p\sqrt{g} g^{ij}$.

2.3 TE/TM decomposition

In our particular case, by considering the wavenumber $k = \omega\sqrt{\varepsilon_0\mu_0}$ and keeping in mind that the contravariant metric tensor g^{ij} does not depend on the variable w , (*i.e.*, $\partial_3 g^{ij} \equiv 0$), it is trivial to obtain a set of six equations:

$$\partial_2 E_3 - \partial_3 E_2 = -ik\mu_0\mu_p (G_1 + g^{13}G_3) \quad (5)$$

$$\partial_3 E_1 - \partial_1 E_3 = -ik\mu_0\mu_p (G_2 + g^{23}G_3) \quad (6)$$

$$\partial_1 E_2 - \partial_2 E_1 = -ik\mu_0\mu_p (g^{13}G_1 + g^{23}G_2 + g^{33}G_3) \quad (7)$$

$$\partial_2 G_3 - \partial_3 G_2 = ik\varepsilon_0\varepsilon_p (E_1 + g^{13}E_3) \quad (8)$$

$$\partial_3 G_1 - \partial_1 G_3 = ik\varepsilon_0\varepsilon_p (E_2 + g^{23}E_3) \quad (9)$$

$$\partial_1 G_2 - \partial_2 G_1 = ik\varepsilon_0\varepsilon_p (g^{13}E_1 + g^{23}E_2 + g^{33}E_3) \quad (10)$$

where \mathbf{G} denotes the magnetic field normalized by the vacuum wave impedance as $\mathbf{G} = \sqrt{\frac{\mu_0}{\varepsilon_0}} \mathbf{H}$. Then, it is possible to choose two potentials which are the longitudinal covariant components of the fields E_3 and G_3 , so from (7) and (10), one can obtain:

$$G_3 = -\frac{1}{ik\mu_0\mu_p} [g^{33}]^{-1} [\partial_1 E_2 - \partial_2 E_1 - g^{13}G_1 - g^{23}G_2] \quad (11)$$

$$E_3 = +\frac{1}{ik\varepsilon_0\varepsilon_p} [g^{33}]^{-1} [\partial_1 G_2 - \partial_2 G_1 - g^{13}E_1 - g^{23}E_2] \quad (12)$$

If we substitute these expressions into (5, 6, 8) and (9), the tangential components of the electromagnetic field are given by [12]:

$$\begin{aligned} (k_c^2 + \partial_3^2) E_1 &= (\partial_1 \partial_3 - k_c^2 g^{13}) E_3 - ik\mu_0\mu_p (\partial_2 + g^{23} \partial_3) G_3 \\ (k_c^2 + \partial_3^2) E_2 &= (\partial_2 \partial_3 - k_c^2 g^{23}) E_3 + ik\mu_0\mu_p (\partial_1 + g^{13} \partial_3) G_3 \\ (k_c^2 + \partial_3^2) G_1 &= ik\varepsilon_0\varepsilon_p (\partial_2 + g^{23} \partial_3) E_3 + (\partial_1 \partial_3 - k_c^2 g^{13}) G_3 \\ (k_c^2 + \partial_3^2) G_2 &= -ik\varepsilon_0\varepsilon_p (\partial_1 + g^{13} \partial_3) E_3 + (\partial_2 \partial_3 - k_c^2 g^{23}) G_3 \end{aligned} \quad (13)$$

with $k_c^2 = k^2 \mu_p \varepsilon_p$. Then, let us introduce the separation of variable so that $\Phi(x^1, x^2, x^3) = \phi(x^1, x^2) \exp^{-i\gamma x^3}$. Thus, the partial derivative operator ∂_3^2 can be substituted by $-\gamma^2$ and provided that $k_c^2 - \gamma^2 \neq 0$, one can obtain the tangential components:

$$\begin{aligned}
E_1 &= \frac{1}{k_c^2 - \gamma^2} [(\partial_1 \partial_3 - k_c^2 g^{13}) E_3 - ik\mu_0 \mu_p (\partial_2 + g^{23} \partial_3) G_3] \\
E_2 &= \frac{1}{k_c^2 - \gamma^2} [(\partial_2 \partial_3 - k_c^2 g^{23}) E_3 + ik\mu_0 \mu_p (\partial_1 + g^{13} \partial_z) G_3] \\
G_1 &= \frac{1}{k_c^2 - \gamma^2} [+ik\varepsilon_0 \varepsilon_p (\partial_2 + g^{23} \partial_z) E_3 + (\partial_1 \partial_3 - k_c^2 g^{13}) G_3] \\
G_2 &= \frac{1}{k_c^2 - \gamma^2} [-ik\varepsilon_0 \varepsilon_p (\partial_1 + g^{13} \partial_z) E_3 + (\partial_2 \partial_z - k_c^2 g^{23}) G_3]
\end{aligned} \tag{14}$$

The above relations show that in homogeneous source-free region, the components of the fields can be expressed as a linear combination of a *TE* field ($E_3 = 0$) and a *TM* field ($G_3 = 0$).

2.4 The eigenvalue problem to solve

The main problem consists in writing any propagation (diffusion) equation which must be satisfied by the two potentials. After some tedious calculations, it is possible to show that the two potentials E_3 and H_3 satisfy the same Helmholtz's equation translated in the new coordinates system [12]:

$$[g^{33} \partial_3^2 + (\partial_1 g^{13} + g^{13} \partial_1) \partial_3 + (\partial_2 g^{23} + g^{23} \partial_2) \partial_3 + \partial_1^2 + \partial_2^2 + k_c^2] \phi = 0 \tag{15}$$

Let us consider the notations $\phi'(x^1, x^2) = \partial_3 \phi(x^1, x^2)$ and $\eta^2 = (\partial_1^2 + \partial_2^2 + k_c^2)$. The wave propagation becomes:

$$-\partial_3 \phi' = (g^{33})^{-1} [(\partial_1 g^{13} + g^{13} \partial_1) + (\partial_2 g^{23} + g^{23} \partial_2)] \phi' + (g^{33})^{-1} \eta^2 \phi \tag{16}$$

An eigenvalue system can be obtained by adding the equation $i\phi' = \gamma\phi$, so:

$$\begin{bmatrix} i\phi' \\ \phi \end{bmatrix} \gamma = \begin{bmatrix} -i(g^{33})^{-1} [(\partial_1 g^{13} + g^{13} \partial_1) + (\partial_2 g^{23} + g^{23} \partial_2)] & (g^{33})^{-1} \eta^2 \\ I_d & 0 \end{bmatrix} \begin{bmatrix} i\phi' \\ \phi \end{bmatrix} \tag{17}$$

In order to progress into the numerical resolution of the problem, it is necessary to choose now any basis functions in order to obtain an algebraic equation to solve the eigenvalue problem (17). This is the purpose of the next section.

2.5 Numerical strategy: projection on basis functions

In order to discretize the differential operators, a 2D-Fourier transform is defined along the directions x^1 and x^2 . The corresponding spatial frequencies are denoted by α and β respectively. The potential $\phi(x^1, x^2, x^3)$ in the spatial domain may be reconstructed from the potential $\hat{\phi}(\alpha, \beta, x^3)$ in the spectral domain:

$$\phi(x^1, x^2, x^3) = \mathcal{TF}^{-1} [\hat{\phi}(\alpha, \beta, x^3)] = \iint_{-\infty}^{+\infty} \hat{\phi}(\alpha, \beta, x^3) e^{-i(\alpha x^1 + \beta x^2)} d\alpha d\beta. \tag{18}$$

Thus, the first eigenvalue system (17) can be translated in the Fourier domain. Considering $\psi = i\phi'$ and by using usual rules in the Fourier domain, one obtains:

$$\begin{bmatrix} \hat{\psi} \\ \hat{\phi} \end{bmatrix} \gamma = \begin{bmatrix} (\hat{g}^{33})^{-1} * [(\alpha * \hat{g}^{13} + \hat{g}^{13} * \alpha) + (\beta * \hat{g}^{23} + \hat{g}^{23} * \beta)] & (\hat{g}^{33})^{-1} * \hat{\eta}^2 \\ I_d & 0 \end{bmatrix} \begin{bmatrix} \hat{\psi} \\ \hat{\phi} \end{bmatrix} \quad (19)$$

where η^2 is also transformed in the Fourier domain $\hat{\eta}^2 = (k_c^2 - \alpha^2 - \beta^2)$ and $*$ denotes the convolution product in the Fourier space. I_d stands for the identity operator. This representation of the potential assumes a continuous Fourier space. In practice, the Fourier space must be discretized and truncated. To do that, we exploit the same explanations as already presented in two previous papers [3] and [13] except it must be generalized to the 2D Fourier space. In summary, let us assume a finite number of harmonics to represent the potential, hence:

$$\phi(x^1, x^2, x^3) = \mathcal{TF}^{-1} \left[\hat{\phi}(\alpha, \beta, x^3) \right] \approx \sum_{m=-M}^{m=+M} \sum_{n=-N}^{n=+N} \hat{\phi}_{mn} e^{-i\alpha_m x^1 - i\beta_n x^2}. \quad (20)$$

The convolution product $(\hat{g} * \hat{\phi})(\alpha, \beta, x^3)$ results in the discrete Fourier space by a matrix product of the form $[\mathbf{g}] \hat{\phi}$ where $\hat{\phi}$ is a column vector resulting from the concatenation of all the discrete values $\hat{\phi}_{mn}$. $[\mathbf{g}]$ is a truncated 2D convolution matrix generated by the column vector resulting from the concatenation of the discrete values \hat{g}_{mn} in the 2D Fourier space. The keystone of this numerical model lies in building all the 2D truncated convolution matrices. Moreover, in Fourier space the derivation is a multiplicative operator $\partial_1 \phi(x^1, x^2, x^3) \xrightarrow{\text{FT}} -i\alpha \hat{\phi}(\alpha, \beta, x^3)$. In truncated 2D spectral domain, the partial derivation with respect to variable x^1 consists operationally in multiplying the approximated solution by a matrix \mathbf{D}_1 such that $\mathbf{D}_1 = -i[\boldsymbol{\alpha}] \otimes \mathbf{I}_{2M+1}$ with $[\boldsymbol{\alpha}] = \text{diag}(\alpha_m)$, \mathbf{I}_{2M+1} the identity matrix of size $2M+1$ and \otimes the kronecker product. In the same way, the matrix associated to the partial derivation with respect to variable x^2 is $\mathbf{D}_2 = -i\mathbf{I}_{2N+1}[\boldsymbol{\beta}]$ with $[\boldsymbol{\beta}] = \text{diag}(\beta_n)$. Finally, we obtain the following eigenvalue algebraic system in the discretized 2D Fourier domain:

$$\begin{bmatrix} \hat{\psi} \\ \hat{\phi} \end{bmatrix} \gamma = \begin{bmatrix} -[\hat{\mathbf{g}}^{33}]^{-1} [\mathbf{D}] & [\hat{\mathbf{g}}^{33}]^{-1} [\hat{\eta}^2] \\ \mathbf{I}_d & 0 \end{bmatrix} \begin{bmatrix} \hat{\psi} \\ \hat{\phi} \end{bmatrix} \quad (21)$$

with $[\hat{\eta}^2] = k_c^2 + \mathbf{D}_1 \mathbf{D}_1 + \mathbf{D}_2 \mathbf{D}_2$ and $[\mathbf{D}] = i\mathbf{D}_1 [\hat{\mathbf{g}}^{13}] + [\hat{\mathbf{g}}^{13}] i\mathbf{D}_1 + i\mathbf{D}_2 [\hat{\mathbf{g}}^{23}] + [\hat{\mathbf{g}}^{23}] i\mathbf{D}_2$. To complete the description of the discrete operators, it is necessary to develop the expressions of the matrices $[\hat{\mathbf{g}}^{ij}]$:

$$[\hat{\mathbf{g}}^{13}] = [\hat{\mathbf{g}}^{31}] = -[\hat{\mathbf{A}}_u] \quad (22)$$

$$[\hat{\mathbf{g}}^{23}] = [\hat{\mathbf{g}}^{32}] = -[\hat{\mathbf{A}}_v] \quad (23)$$

$$[\hat{\mathbf{g}}^{33}] = \mathbf{I}_d + [\hat{\mathbf{g}}^{13}] [\hat{\mathbf{g}}^{13}] + [\hat{\mathbf{g}}^{23}] [\hat{\mathbf{g}}^{23}] \quad (24)$$

where $[\hat{\mathbf{A}}_1]$ and $[\hat{\mathbf{A}}_2]$ stand for the convolution matrices associated with the Fourier transforms $\mathcal{TF}(\dot{a}_1)$ and $\mathcal{TF}(\dot{a}_2)$ respectively. One can note also that $[\hat{\mathbf{g}}^{33}]^{-1}$ is the inverse matrix of $[\hat{\mathbf{g}}^{33}]$.

2.6 Modal expansion of the potentials

For each medium p , the numerical eigensolutions of equation (19) provides a modal expansion of the two scalar potentials E_3 and G_3 :

$$\begin{aligned}\widehat{E}_3^{(p)} &= \sum_q \psi_q^{(p+)} \Gamma_q^{TE(p+)} e^{-i\gamma_q^{(p+)} x^3} + \sum_q \psi_q^{(p-)} \Gamma_q^{TE(p-)} e^{-i\gamma_q^{(p-)} x^3} \\ \widehat{G}_3^{(p)} &= \sum_q \psi_q^{(p+)} \Gamma_q^{TM(p+)} e^{-i\gamma_q^{(p+)} x^3} + \sum_q \psi_q^{(p-)} \Gamma_q^{TM(p-)} e^{-i\gamma_q^{(p-)} x^3}\end{aligned}\quad (25)$$

where $\psi_q^{(p)\pm}$ denotes the eigenvectors associated to the eigenvalues $\gamma_q^{(p)\pm}$. The unknown coefficients are $\Gamma_q^{TE(p)\pm}$ and $\Gamma_q^{TM(p)\pm}$. The forward the backward contributions of the field differ from the sign \pm of the exponents and non-physical solutions (growing towards infinity) are suppressed.

2.7 Particular case: the half-space

In the particular case where the rough surface separates two half-spaces, let us denote the air domain $p = 0$ and the conductor $p = 1$. In order to guaranty the decreasing of the field in each domain, the expansion of the field involves only two eigensolutions: $\psi_q^{(0+)}$ corresponding to $\Im(\gamma_q^{(0+)}) < 0$ and $\psi_q^{(1-)}$ corresponding to $\Im(\gamma_q^{(1-)}) > 0$. Moreover, at the interface $x^3 = 0$, the two vectors $\widehat{\mathbf{E}}_3^{(p)}$ and $\widehat{\mathbf{G}}_3^{(p)}$ which are resulting from the concatenation of all its numerical values in the 2D Fourier space can be obtained by two matrix relationships. Without taking into account the incident field at this step, the contributions of the fields due to the slab are given by:

$$\begin{aligned}\widehat{\mathbf{E}}_3^{(0)} &= \boldsymbol{\psi}^{(0+)} \boldsymbol{\Gamma}^{TE(0+)}, & \widehat{\mathbf{G}}_3^{(0)} &= \boldsymbol{\psi}^{(0+)} \boldsymbol{\Gamma}^{TM(0+)}, & \text{in air} \\ \widehat{\mathbf{E}}_3^{(1)} &= \boldsymbol{\psi}^{(1-)} \boldsymbol{\Gamma}^{TE(1-)}, & \widehat{\mathbf{G}}_3^{(1)} &= \boldsymbol{\psi}^{(1-)} \boldsymbol{\Gamma}^{TM(1-)}, & \text{in the conductor.}\end{aligned}\quad (26)$$

The discrete versions of equations (14) gives the expansions of the tangential components of the electromagnetic field at the interface $x^3 = 0$, so for the field vectors:

$$\begin{bmatrix} \widehat{\mathbf{E}}_2^{(p)} \\ \widehat{\mathbf{G}}_1^{(p)} \\ \widehat{\mathbf{G}}_2^{(p)} \\ \widehat{\mathbf{E}}_1^{(p)} \end{bmatrix} = \begin{bmatrix} +ik\mu_0\mu_p \mathcal{M}_p^\pm \\ \mathcal{O}_p^\pm \\ \mathcal{N}_p^\pm \\ -ik\mu_0\mu_p \mathcal{P}_p^\pm \end{bmatrix} \boldsymbol{\Gamma}^{TE(p\pm)} + \begin{bmatrix} \mathcal{N}_p^\pm \\ +ik\varepsilon_0\varepsilon_p \mathcal{P}_p^\pm \\ -ik\varepsilon_0\varepsilon_p \mathcal{M}_p^\pm \\ \mathcal{O}_p^\pm \end{bmatrix} \boldsymbol{\Gamma}^{TM(p\pm)}\quad (27)$$

The operators are given by:

$$\begin{aligned}\mathcal{M}_p^\pm &= \mathbf{D}_1 \boldsymbol{\psi}^{(p\pm)} \left[\mathbf{D}_\lambda^{(p\pm)} \right]^{-1} + [\hat{\mathbf{g}}^{13}] \boldsymbol{\psi}^{(p\pm)} \left[\mathbf{D}_\lambda^{(p\pm)} \right]^{-1} \mathbf{D}_3^{(p\pm)} \\ \mathcal{N}_p^\pm &= \mathbf{D}_2 \boldsymbol{\psi}^{(p\pm)} \left[\mathbf{D}_\lambda^{(p\pm)} \right]^{-1} \mathbf{D}_3^{(p\pm)} - k_c^2 [\hat{\mathbf{g}}^{23}] \boldsymbol{\psi}^{(p\pm)} \left[\mathbf{D}_\lambda^{(p\pm)} \right]^{-1} \\ \mathcal{O}_p^\pm &= \mathbf{D}_1 \boldsymbol{\psi}^{(p\pm)} \left[\mathbf{D}_\lambda^{(p\pm)} \right]^{-1} \mathbf{D}_3^{(p\pm)} - k_c^2 [\hat{\mathbf{g}}^{13}] \boldsymbol{\psi}^{(p)} \left[\mathbf{D}_\lambda^{(p)} \right]^{-1} \\ \mathcal{P}_p^\pm &= \mathbf{D}_2 \boldsymbol{\psi}^{(p\pm)} \left[\mathbf{D}_\lambda^{(p\pm)} \right]^{-1} + [\hat{\mathbf{g}}^{23}] \boldsymbol{\psi}^{(p\pm)} \left[\mathbf{D}_\lambda^{(p\pm)} \right]^{-1} \mathbf{D}_3^{(p\pm)}\end{aligned}\quad (28)$$

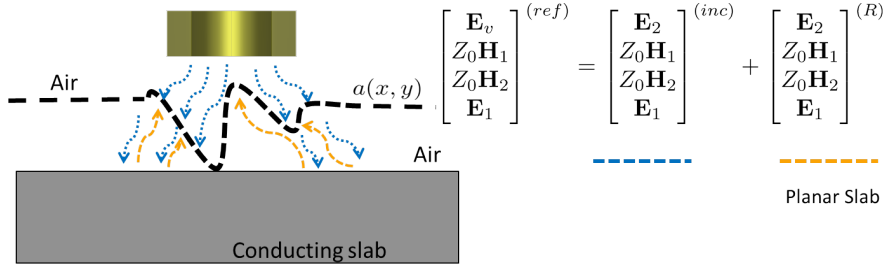


Figure 2: The 3D EC probe is scanning a conductive planar slab for computing the reference field.

with $\mathbf{D}_3^{(0+)} = -i\gamma^{(0+)}$ and $\mathbf{D}_3^{(1-)} = -i\gamma^{(1-)}$ are two diagonal matrices constituted by all eigenvalues in the region $p \in \{0, 1\}$. $\mathbf{D}_\gamma^{(p\pm)}$ is also a diagonal matrix constituted by all values $k_c^2 - [\gamma^{(p\pm)}]^2$ in the region $p \in \{0, 1\}$. The matrices $\mathcal{M}_p^\pm, \mathcal{N}_p^\pm, \mathcal{O}_p^\pm$ and \mathcal{P}_p^\pm correspond to the operators associated to the progressive or regressive coefficients in both air ($p = 0$) and conductor ($p = 1$). The vectors $\mathbf{\Gamma}^{TE(p\pm)}$ and $\mathbf{\Gamma}^{TM(p\pm)}$ of unknown coefficients are then estimated by applying boundary conditions.

2.8 Boundary conditions for the half-space

The continuity of each tangential component of the electromagnetic field must be satisfied at the interface air-conductor. Indeed, at the rough surface $w = 0$, the electromagnetic field at the surface is the sum of a reference field provided by any EC probe and a reflected field due to the presence of the conductive slab. Since, the electromagnetic field must be evaluated at $w = 0$, the values of reference field must be calculated on the rough surface. The reference configuration may be however arbitrary chosen, so we choose to consider an EC probe scanning a conducting plate of finite thickness, the planar slab is located at the lowest point of the surface. This point is illustrated on a slice view in figure 2. Since the two conditions $k_c^2 - [\gamma^{(0+)}]^2 \neq 0$ and $k_c^2 - [\gamma^{(1-)}]^2 \neq 0$ are satisfied both together, the first set of boundary conditions can be written in a matrix form in the Fourier domain so that:

$$\begin{bmatrix} ik\mu_0\mu_1 \mathcal{M}_0^+ & \mathcal{N}_0^+ & -ik\mu_0\mu_2 \mathcal{M}_1^- & -\mathcal{N}_1^- \\ \mathcal{O}_0^+ & +ik\varepsilon_0\varepsilon_1 \mathcal{P}_0^+ & -\mathcal{O}_1^- & -ik\varepsilon_0\varepsilon_2 \mathcal{P}_1^- \\ \mathcal{N}_0^+ & -ik\varepsilon_0\varepsilon_1 \mathcal{M}_0^+ & -\mathcal{N}_1^- & +ik\varepsilon_0\varepsilon_2 \mathcal{M}_1^- \\ -ik\mu_0\mu_1 \mathcal{P}_0^+ & \mathcal{O}_0^+ & +ik\mu_0\mu_2 \mathcal{P}_1^- & -\mathcal{O}_1^- \end{bmatrix} \begin{bmatrix} \mathbf{\Gamma}^{TE(0+)} \\ \mathbf{\Gamma}^{TM(0+)} \\ \mathbf{\Gamma}^{TE(1-)} \\ \mathbf{\Gamma}^{TM(1-)} \end{bmatrix} = - \begin{bmatrix} \hat{\mathbf{E}}_2^{(ref)} \\ \hat{\mathbf{G}}_1^{(ref)} \\ \hat{\mathbf{G}}_2^{(ref)} \\ \hat{\mathbf{E}}_1^{(ref)} \end{bmatrix} \quad (29)$$

where the terms $\hat{\mathbf{E}}_{1,2}^{(ref)}$ and $\hat{\mathbf{G}}_{1,2}^{(ref)}$ are the Fourier transforms of the tangential components of the reference field. The resolution of this system by a direct matrix inversion leads to the computation of the coefficients in both media.

2.9 Computation of the impedance of the probe

The most usual way to compute the the response of the EC probe, the electrical impedance ΔZ consists in using the reciprocity principle and the formula derived by Auld and Moulder [14, 15]:

$$I^2 \Delta Z = \iint_{S_F} (\mathbf{E}_a \times \mathbf{H}_b - \mathbf{E}_b \times \mathbf{H}_a) \cdot \mathbf{n} \, ds \quad (30)$$

where I denotes the amplitude of the driving current in the coil. The subscript a and b stand for indicating two different states. The first one can represent the configuration of reference previously discussed, the EC probe scanning a conducting planar slab while the second one refers to the EC probe scanning the rough surface itself. S_F is an arbitrary closed surface bounding the workpiece but excluding the coil (see Figure 3), \mathbf{n} is the unit outward normal with respect to the closed surface S_F . For this geometry, S_F is chosen to be a surface which fits the interface air-conductor considering an

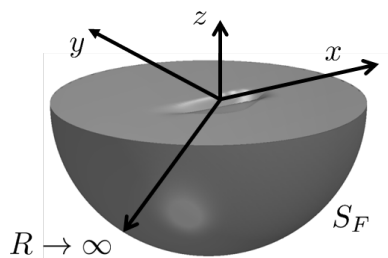


Figure 3: Definition of the closed surface S_F .

infinitesimal distance over the top surface of the workpiece and all the workpiece is enclosed if we consider an hemisphere as shown in Figure 3. In the limit of R tending to infinity, the contribution to this surface S_∞ tends to zero. In Equation (30), the surface S_F can be just substituted by the 2D rough surface denoted by S supported by the profile $a(x, y)$. Into the new coordinates system, this formula becomes:

$$I^2 \Delta Z = \iint_{-\infty}^{+\infty} \left(E_1^{(ref)}(x^1, x^2) H_2(x^1, x^2) - E_2^{(ref)}(x^1, x^2) H_1(x^1, x^2) \right) dx^1 dx^2 \quad (31)$$

To conclude about the theoretical aspects, the tangential components of the field need to be numerically estimated to deduce the change in the impedance of the EC probe. The numerical integration may be performed easily by using a trapezoidal rule. To obtain the absolute impedance, it is necessary to sum the result ΔZ with the impedance of the planar configuration calculated by the same semi-analytical model used for the computation of the reference fields.

3 Numerical results and discussion

Before the presentation of numerical results, it is necessary to discuss about the numerical inversion of the system (29). Indeed, the matrix to invert may be ill-conditioned when any of two terms

$T_p = k_c^2 - [\gamma^{(p\pm)}]^2$, $p \in \{0, 1\}$ are close to zero. The purpose of the following section is to discuss about this specific key point of the numerical model.

3.1 Regularization of the problem

Even if the two terms $T_1 = k_c^2 - [\gamma^{(0+)}]^2$ and $T_2 = k_c^2 - [\gamma^{(1-)}]^2$ cannot be equal to zero, in practice, the condition number of the matrix to invert strongly depends on the closeness of these terms to zero. Thus, any additional treatment must be added to address this situation. In the particular case where $k_c^2 - \gamma^2 = 0$, equations (5, 6, 7, 8, 9, 10) lead to a set of four equations:

$$\begin{aligned} \partial_3 E_2 &= +ik\mu_0\mu_p G_1, & \partial_3 E_1 &= -ik\mu_0\mu_p G_2 \\ \partial_3 G_2 &= -ik\varepsilon_0\varepsilon_p E_u, & \partial_3 G_1 &= +ik\varepsilon_0\varepsilon_p E_2 \end{aligned} \quad (32)$$

and we have to choose another TEM decomposition. The first polarization consists in $E_2 = 0$ and $G_1 = 0$. Knowing that $\gamma = k_c = \pm k^2 \mu_p \varepsilon_p$ and since $\partial_3 E_1 = -i\gamma E_1$, we must satisfy $G_2 = \pm \sqrt{\frac{\varepsilon_0 \varepsilon_p}{\mu_0 \mu_p}} E_1$. The two last equations in (32) are automatically satisfied. For the second polarization, let us consider $E_1 = 0$ and $G_2 = 0$. In this case, we must satisfy the relationship $G_1 = \mp \sqrt{\frac{\varepsilon_0 \varepsilon_p}{\mu_0 \mu_p}} E_2$. In summary, when $k_c^2 - [\gamma^{(p\pm)}]^2 = 0$, the TEM decomposition is given by:

$$\begin{bmatrix} \widehat{\mathbf{E}}_2^{(p)} \\ \widehat{\mathbf{G}}_1^{(p)} \\ \widehat{\mathbf{G}}_2^{(p)} \\ \widehat{\mathbf{E}}_1^{(p)} \end{bmatrix} = \begin{bmatrix} \psi^{(p\pm)} \\ \mp \sqrt{\frac{\varepsilon_0 \varepsilon_p}{\mu_p}} \psi^{(p\pm)} \\ 0 \\ 0 \end{bmatrix} \mathbf{\Gamma}^{TE(p\pm)} + \begin{bmatrix} 0 \\ 0 \\ \pm \sqrt{\frac{\varepsilon_0 \varepsilon_p}{\mu_p}} \psi^{(p\pm)} \\ \psi^{(p)} \end{bmatrix} \mathbf{\Gamma}^{TM(p\pm)} \quad (33)$$

In practice, a threshold t_0 is chosen in order to combine the two TE/TM decompositions. For each media, the eigenvalues $\gamma^{(0+)}$ and $\gamma^{(1-)}$ are ordered in ascending order. According to the value of t_0 , the two conditions $|k_c^2 - [\gamma^{(0+)}]^2| \leq t_0$ and $|k_c^2 - [\gamma^{(1-)}]^2| \leq t_0$ may be satisfied simultaneously or separately. When $|k_c^2 - [\gamma^{(0+)}]^2| \leq t_0$, the TE/TM decomposition (27) is substituted by the TEM decomposition (33). So, we have to solve the following system:

$$\begin{bmatrix} -\psi^{(0+)} & 0 & +ik\mu_0\mu_2 \mathcal{M}_1^- & \mathcal{N}_1^- \\ \pm \sqrt{\frac{\varepsilon_0 \varepsilon_1}{\mu_0 \mu_1}} \psi^{(0+)} & 0 & \mathcal{O}_1^- & +ik\varepsilon_0\varepsilon_2 \mathcal{P}_1^- \\ 0 & \mp \sqrt{\frac{\varepsilon_0 \varepsilon_1}{\mu_0 \mu_1}} \psi^{(0\pm)} & \mathcal{N}_1^- & -ik\varepsilon_0\varepsilon_2 \mathcal{M}_1^- \\ 0 & -\psi^{(0+)} & -ik\mu_0\mu_2 \mathcal{P}_1^- & \mathcal{O}_1^- \end{bmatrix} \begin{bmatrix} \mathbf{\Gamma}^{TE(0+)} \\ \mathbf{\Gamma}^{TM(0+)} \\ \mathbf{\Gamma}^{TE(1-)} \\ \mathbf{\Gamma}^{TM(1-)} \end{bmatrix} = - \begin{bmatrix} \widehat{\mathbf{E}}_2^{(ref)} \\ \widehat{\mathbf{G}}_1^{(ref)} \\ \widehat{\mathbf{G}}_2^{(ref)} \\ \widehat{\mathbf{E}}_1^{(ref)} \end{bmatrix} \quad (34)$$

Moreover, when the condition $|k_c^2 - [\gamma^{(1-)}]^2| \leq t_0$ is simultaneously satisfied, we have to solve the simplified system:

$$\begin{bmatrix} \psi^{(0+)} & 0 & -\psi^{(1-)} & 0 \\ \mp \sqrt{\frac{\varepsilon_0 \varepsilon_1}{\mu_0 \mu_1}} \psi^{(0+)} & 0 & \pm \sqrt{\frac{\varepsilon_0 \varepsilon_2}{\mu_0 \mu_2}} \psi^{(1-)} & 0 \\ 0 & \pm \sqrt{\frac{\varepsilon_0 \varepsilon_1}{\mu_0 \mu_1}} \psi^{(0+)} & 0 & \mp \sqrt{\frac{\varepsilon_0 \varepsilon_2}{\mu_0 \mu_2}} \psi^{(1-)} \\ 0 & \psi^{(0+)} & 0 & -\psi^{(1-)} \end{bmatrix} \begin{bmatrix} \Gamma^{TE(0+)} \\ \Gamma^{TM(0+)} \\ \Gamma^{TE(1-)} \\ \Gamma^{TM(1-)} \end{bmatrix} = - \begin{bmatrix} \widehat{\mathbf{E}}_2^{(ref)} \\ \widehat{\mathbf{G}}_1^{(ref)} \\ \widehat{\mathbf{G}}_2^{(ref)} \\ \widehat{\mathbf{E}}_1^{(ref)} \end{bmatrix} \quad (35)$$

Depending on the value of the threshold t_0 , the reciprocal condition number of the matrix can be evaluated. Figure 4 displays the change in the condition number versus the value of the threshold. According to the value of t_0 , the system to solve may be (29, 34) or (35). When the value of t_0 is too

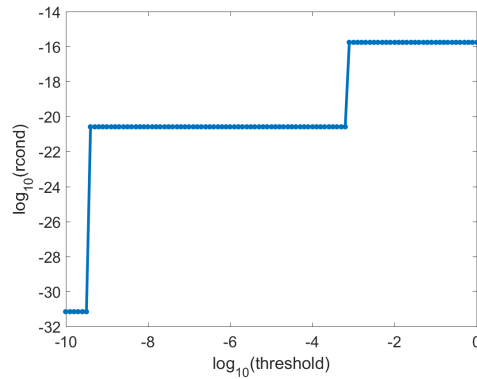


Figure 4: Variations of the reciprocal condition number of the matrix to be inverted. A well conditioned matrix gives a reciprocal condition number near to 1.

low, for the two first levels represented in Fig. 4, the results are not satisfactory and the numerical model does not give quite good results. If the value of t_0 is greater than 10^{-3} , the numerical model can provide quite good results. In this case, only the two equations (29) and (35) are used and then, from the evaluation of the coefficients $\Gamma^{TE(0+)}$, $\Gamma^{TM(0+)}$, $\Gamma^{TE(1-)}$ and $\Gamma^{TM(1-)}$, the tangential components of the field are reconstructed in the spatial domain before deducing the change in the impedance. The impedance due to the reference planar configuration is added to obtain the total absolute impedance of the probe. The next following section gives some numerical results of validation.

4 First validation case of the numerical model

For a first numerical validation, a very simple test configuration have been considered: a conducting half-space is inspected by an air-core EC probe. Such a kind of schematic view of the scene is displayed in Fig. 5. The 2D wavy shape function is assumed to be the product of two cosine functions of the

form such as $a(x, y) = h_p a(x) a(y)$ with:

$$a(s) = \frac{1}{2} \left[1 + \cos \left(2\pi \frac{s}{L_s} \right) \right], \forall s \in [-L_s/2, L_s/2], s = x \text{ or } y$$

This particular surface function has been chosen for its smoothness, but any analytical function can be chosen, as long as the Fourier transform of its first derivative is numerically tractable. The EC probe considered here is a cylindrical pancake coil with a rectangular cross section. For this first configuration, the probe is scanning the geometrical perturbation with a constant altitude. The other parameters required for this numerical experiment are stored in table 1.

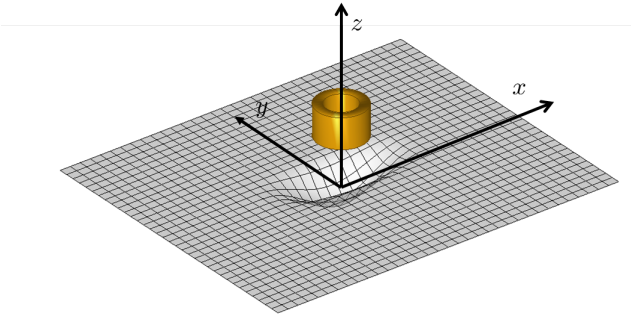


Figure 5: A schematic view of the configuration considered for the numerical validation.

Parameter	symbol	value
Conductor		
Conductivity	σ	1 MS/m
Depth of the flaw	h_p	-2 mm
Length of the shape (x)	L_x	10 mm
Length of the shape (y)	L_y	10 mm
Probe		
Frequency	f	100 kHz
driving current	I_0	1 A
Internal radius	r_{int}	1.0 mm
External radius	r_{ext}	1.6 mm
Height	H	2 mm
Number of turns	N	328
Lift-off	l_0	0.3 mm

Table 1: Simulation parameters.

In order to obtain simulated data for any comparison of the fields, this 3D configuration has been also implemented in a commercial finite element software and the computation of the tangential components of \mathbf{E} and \mathbf{H} have been carried out at the interface $x^3 = 0$. To treat this particular configuration, we fixed the numerical parameters M and N to 23 and 21 respectively. In Fig. 6, the two tangential components of the electrical field obtained with the two numerical methods are represented. For each cartography, a slice view is also displayed in Fig. 7 along the axis of interest. We can see a very good agreement and the same comparison can be made with the same components of \mathbf{H} .

Moreover, the longitudinal component H_3 is also represented in Fig. 8 with two cross section in Fig. 9. In order to complete the numerical validation of the semi-analytical approach, we have also computed the response of the probe (Impedance) for the two methods. These simulated data are represented in Fig. 10. When the probe is sufficiently far from the local perturbation, the impedance tends to the value which corresponds to a planar case. This value can be otherwise obtained rigorously by the civa software. This value is also displayed on the curves. The very small discrepancy between

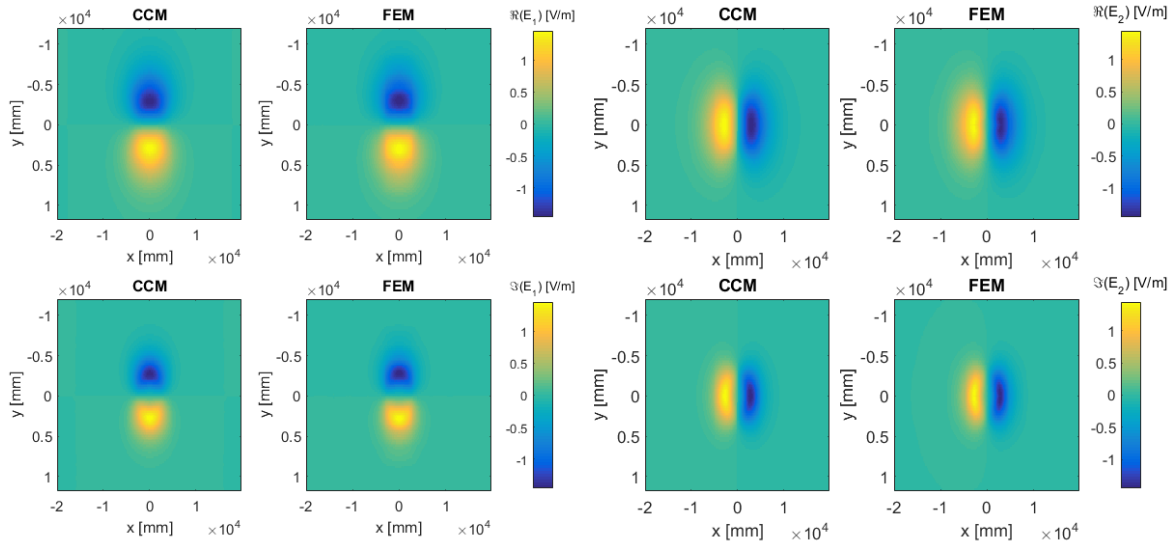


Figure 6: Comparison of the tangential components of \mathbf{E} provided by the C method (CCM) or by Finite Element (FE). On the top, cartographies of real parts are displayed, imaginary parts are placed at the bottom.

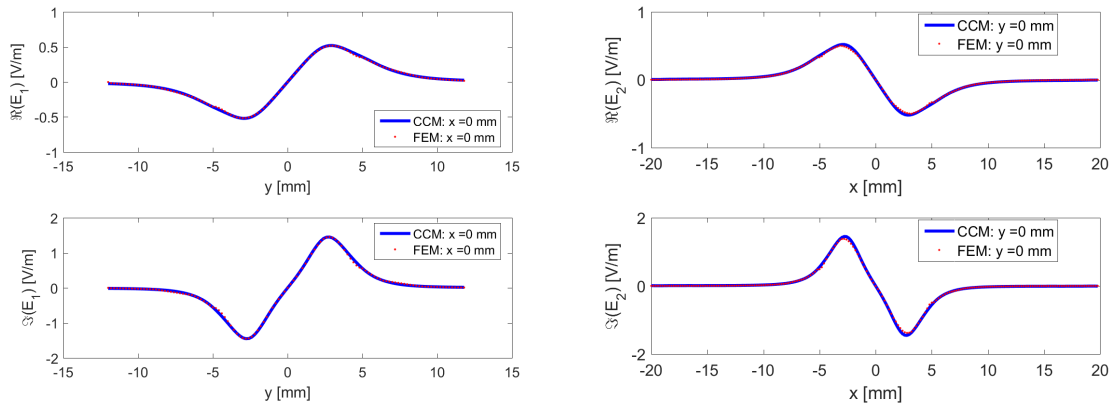


Figure 7: A sliceview of the comparison of the tangential components of \mathbf{E} provided by CCM or by FE.

the FEM model and the CCM model is quantified by the normalized root mean square error defined

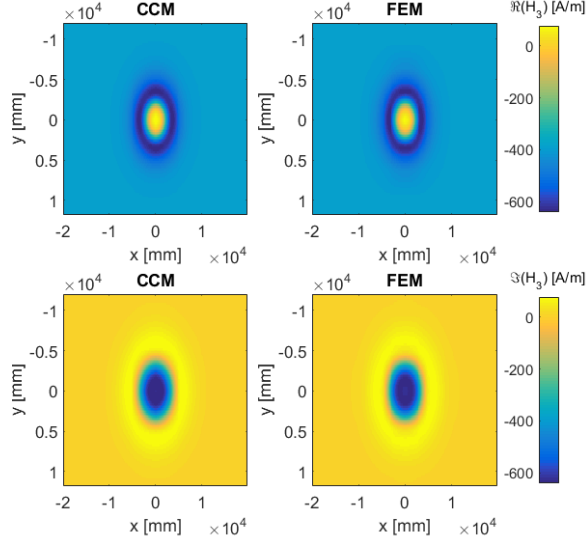


Figure 8: Comparison of the longitudinal component of H_w provided by CCM or by FE. On the top, cartographies of real parts are displayed, imaginary parts are placed at the bottom.

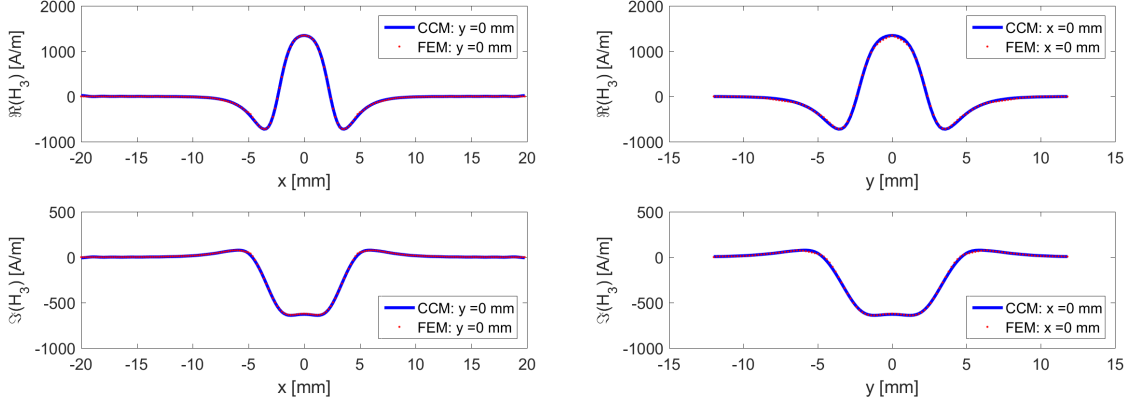


Figure 9: A sliceview of the comparison of the longitudinal component of H_w provided by CCM or by FE. On the top, cartographies of real parts are displayed, imaginary parts are placed at the bottom.

separately on the real part and on the imaginary part:

$$\varepsilon_R = \sqrt{\frac{\|\Re(\tilde{Z}_{CCM} - Z_{EF})\|^2}{\|\Re(Z_{EF})\|^2}}, \quad \varepsilon_X = \sqrt{\frac{\|\Im(\tilde{Z}_{CCM} - Z_{EF})\|^2}{\|\Im(Z_{EF})\|^2}} \quad (36)$$

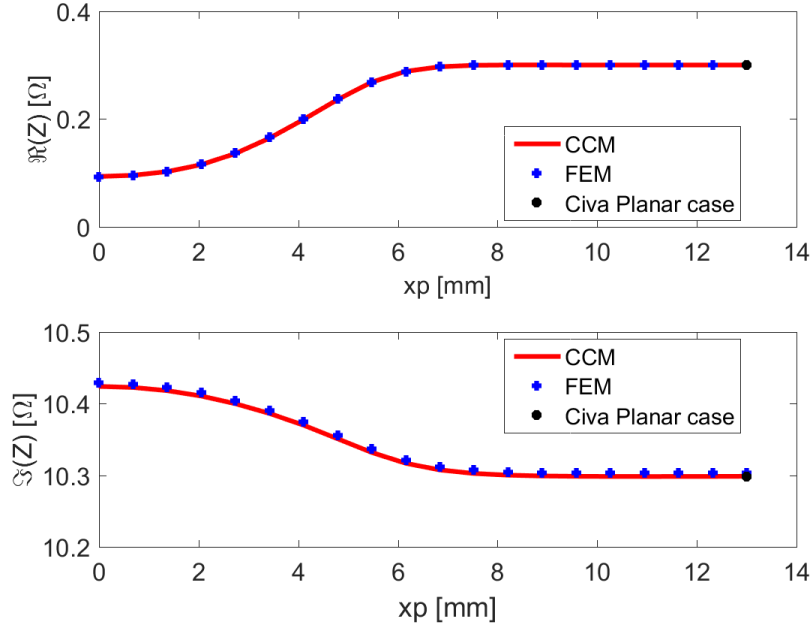


Figure 10: Comparison of the probe response obtained with the CCM and the Finite Element method. The errors are evaluated to $\varepsilon_R < 0.3\%$ and $\varepsilon_X < 0.05\%$.

The computational time obtained with CCM in this particular configuration on a 64-bits platform is about 9 mn without including the computation of the incident fields which are already done by another model already implemented into the CIVA software [16]. This value represents the full time necessary to compute the eigenfunctions and the solutions for all the positions of the sensor. Nevertheless, if another scan of the EC probe must be considered, the computational time is reduced since the eigenfunctions have been already computed. The most consuming time computation lies in the resolution of the eigenvalue problem. Moreover, this time computation depends on the orders of truncation in the Fourier domain. This truncation constitutes the real limitation of the numerical model today because it leads to a large matrix when solving in particular the matrix equation (29). Another complementary algorithms will be implemented to overcome this limitation in order to be able to increase the number of modes according to the two directions X and Y . In contrary, the increasing of the number of layers is not really a limitation since the S-matrix algorithm [17, 18, 5] will be implemented in the future. In order to simulate this investigated NDT configuration, an half-geometry has been considered in the FE software in order to reduce as much as possible the number of elements and the size of the problem in the memory space. Even if the parameters L_x and L_y have been chosen to be equal in this configuration, the function $a(x, y)$ resulting from the product of the two functions $a(x)$ and $a(y)$ leads to construct a real 3D surface which does not present any symmetry except along the

Y axis. This particular configuration has been chosen in order to be allowed to address more easily this 3D problem by using a commercial FE software. In practice, the limitation of the FE solver has been almost reached due to the number of elements for obtaining a satisfying accuracy. However, no symmetry has been used for solving the 3D case by the CCM method. Moreover, in the general case, when the pancake coil is scanning the 3D surface, the problem to solve is a full 3D one.

5 Conclusion

In this paper, a new 3D numerical model based on the covariant form of Maxwell's equation is proposed for the first time in order to develop any simulation tools for the virtual inspection of a conductor slab of complex shape. This fast semi-analytical 3D model is dedicated today to the computation of eddy currents induced by a 3D sensor (with no interacting part such as ferrite or shielding) in a conducting half space but the formalism gives a key starting point for solving efficiently more complex situations in the future. The single interface air-conductor is characterized by a 3D arbitrary surface described by a 2D analytic function $a(x, y)$. In a clever new system of coordinates, tangential components of the electromagnetic field are expressed from two longitudinal components of the field E_3 and H_3 . These two components both satisfy a wave equation which depends on the geometry of the rough surface by including several coefficients of the metric tensor. By using Fourier basis functions, the wave equation is translated in an algebraic equation which can provide eigensolutions of the structure. The two longitudinal components of the field are then expanded in series of modal solutions and the coefficients of the series are evaluated by satisfying the boundary condition at the interface. The main advantage of this approach lies in the fact that the boundary condition can be written analytically without requiring any mesh. Once the coefficients of the modal expansion are evaluated, the tangential components of the field are reconstructed in the spatial domain in order to compute the response of the EC probe. The numerical implementation coming from this formalism in the Fourier Domain leads particularly to an efficient computation of the response of the sensor even if there is a great number of points during the scan. Thanks to this 3D formalism, this 3D numerical model will be extended relatively easily to stratified media by implementing the S-matrix algorithm which has been previously and successfully implemented [5, 6] for 2D geometries of the workpiece. This is the main extension of the code we expect to develop in the future. Nevertheless, this model presents some drawbacks which must be overcome: in particular the number of modes. Indeed, the size of the eigenproblem to solve strongly depends on the number of modes in the expansion. The limitation in the memory space can have an impact today on the roughness of the 3D surface. Some developments will be necessary to overcome this difficulty. A convergence study will be addressed in a future paper depending on the roughness of the profile. Nevertheless, some 3D NDT geometries of interest can be addressed today without applying any symmetry condition as this is the case for the FE method. The time computation remains relatively short in comparison to FE computations. The accuracy of the model is also satisfying without increasing the number of modes since the convergence of the method is starting to be reached. The choice of other basis functions such as splines [19] is already envisaged in order to reduce drastically the number of modes which are necessary for the description of the fields

and the 3D profile.

References

- [1] J. Chandezon *et al.*, *A new theoretical method for diffraction gratings and its numerical application*, in *Journal of Optics*, vol. 11, pp. 235, 1980.
- [2] K.A. Braham and R. Dusséaux and G. Granet, *Scattering of electromagnetic waves from two-dimensional perfectly conducting random rough surfaces-study with the curvilinear coordinate method*, in *Waves in Random and Complex Media*, vol. 18 2, pp. 255-274.
- [3] D. Prémel, *Computation of a quasi-static field induced by two long straight parallel wires in a conductor with a rough surface*, in *Journal of Physics D: Applied Physics*, vol. 41, no. 245305, 2008.
- [4] F. Caire, D.Prémel and G.Granet, *Semi-analytical computation of a quasi-static field induced by an eddy current probe in a conductor with a rough surface*, *The European Physics Journal Applied Physics*, vol. 64, 2013.
- [5] F. Caire, D. Prémel, and G. Granet, *Semi-analytical computation of a quasi-static field induced by a 3D eddy current probe scanning a 2D layered conductor with parallel rough interfaces*, *International Journal of Numerical Modelling: Electronic Networks, Devices and Fields*, vol. 27, no.3, pp. 600–613, 2014.
- [6] F. Caire, D. Prémel, and G. Granet, *Fast Computation of the Fields Diffracted by a Multi-Layered Conductor With Non-Parallel Rough Interfaces. Application to Eddy-Current Non-Destructive Testing Simulation*, *IEEE Transaction on magnetics*, vol. 51, no.3, pp. 6200604, 2015.
- [7] D. Prémel, *Generalization of the Second Order Vector Potential Formulation for Arbitrary Non-Orthogonal Curvilinear Coordinates Systems from the Covariant Form of Maxwell's Equations*, *Journal of Electromagnetic Analysis and Applications*, vol. 4, pp. 400-409, 2012.
- [8] A. Skarlatos, E. Demaldent, A. Vigneron, C. Reboud, *Modelling of specimen interaction with ferrite cored coils by coupling semi-analytical and numerical techniques*, *Series Studies in Applied Electromagnetics and Mechanics, Electromagnetic Nondestructive Evaluation (XVII)*, vol. 39, pp. 128-135, 2014.
- [9] E. Post, *Formal structure of electromagnetics: General covariance and electromagnetics*, Amsterdam: North-Holland, 1962.
- [10] A. Nicolet and F. Zolla and Y. Ould Agha and S. Guenneau, *Geometrical transformations and equivalent materials in computational electromagnetism*, *COMPEL - The international journal for computation and mathematics in electrical and electronic engineerin*, vol. 27, no. 4, pp. 806-819, 2008.

- [11] J.P. Plumey, B. Guizal and J. Chandezon, *The coordinate transformation method as applied to asymmetric gratings with vertical facets*, Journal of the Optical Society of America A, vol. 14, no. 3, pp. 610-617, 1997.
- [12] G. Granet, *Analysis of diffraction by surface-relief crossed gratings with use of the Chandezon method: application to multilayer crossed gratings*, J. Opt. Soc. Am. A, vol. 15, no. 5, pp. 1121-1131, 1998.
- [13] D. Prémel and G. Granet and F. Caire, *Matching curvilinear coordinates for the computation of the distribution of eddy currents in a cylindrical tube described by an arbitrary longitudinal internal/external profile*, Eur. Phys. J. Appl. Phys., vol. 73, no. 1, pp. 10903, 2016.
- [14] B.A. Auld and J.C. Moulder, *Review of Advances in Quantitative Eddy Current*, Journal of Nondestructive Evaluation, vol. 18, no. 1, pp. 3-36, 1999.
- [15] S.K. Burke and M.E. Ibrahim, *Mutual impedance of air-cored coils above a conducting plate*, Journal of Physics D: Applied Physics, vol. 37, no. 13, pp. 1857-1868, 2004.
- [16] C. Reboud and T. Theodoulidis, *Field computations of inductive sensors with various shapes for semi-analytical ECT simulation*, Studies in Applied Electromagnetics and Mechanics, vol. 36, pp. 3-10, 2012.
- [17] N. P. K. Cotter *et al.*, *Scattering-matrix approach to multilayer diffraction*, J. Opt. Soc. Am., vol. 12, pp. 1097-1103, 1995.
- [18] L. Li, *Formulation and comparison of two recursive matrix algorithms for modeling layered diffraction gratings*, J. Opt. Soc. Am. A, vol. 13, no. 5, May 1996.
- [19] Gérard Granet, *Efficient implementation of B-spline modal method for lamellar gratings*, J. Opt. Soc. Am. A, vol. 31, no. 2, pp. 332-337, 2014.